scattered sunlight. Derive the degree of circular polarization of this sunlight due to single scattering by these particles.

5.12. Derive (5.72).

5.13. The volume backscattering coefficient β (this has units of inverse length and the relation between this coefficient and the radar reflectivity is explored in Chapter 8) for a volume filled with N_o identical cloud drops is defined as [see (5.65)]

$$\beta = N_o C_b.$$

a. Show that for spherical Rayleigh scatterers of radius a,

$$\beta = N_o \frac{64\pi^5}{\lambda^4} a^6 \mid K \mid^2$$

b. Assuming that the number density and radius of cloud droplets are 100 cm^{-3} and 20 μm, respectively, calculate β for the following two wavelengths (see table) where m is the refractive index of water. Repeat these calculations for raindrops that are 1 mm in size and with a concentration of $N_o = 1$ $liter^{-1}$.

Wavelength (cm)	10	3.21
m= (n, κ)	(3.99,1.47)	(7.14,2.89)

6
Passive Sensing — Extinction and Scattering

The preceding four chapters describe different aspects of how electromagnetic radiation interacts with matter. Most practical applications, however, rely on measurements of the accumulated effect of many interactions not a single interaction. The actual path along which these interactions occur might be just a few meters in some cases or hundreds of kilometers for instruments on meteorological satellites. Some way of describing the accumulated effects of all processes as radiation is transferred from one volume of atmosphere to another along these paths is needed.

The theory of radiative transfer provides such a description and two special forms of radiative transfer are introduced in this chapter. One treats only extinction and examples of remote sensing of path integrated quantities based on measurements of this extinction are discussed in the following two sections. The problem of radiative transfer in an opaque scattering atmosphere is unfortunately not described by this extinction equation. In dense media, like clouds, photons reappear along a given direction because of multiple scattering. Accounting for these scattered photons complicates the radiative transfer and ways of simplifying this complexity are discussed in the context of the remote sensing of aerosol, ozone, and clouds.

6.1 Beer's Law and the Remote Sensing of Aerosol

Lambert's law of extinction, introduced in Chapter 3, states that the change in the intensity of radiation emerging from the end of a path of length ds is proportional to the incoming intensity, namely

$$dI_\lambda = -\sigma_{ext,\lambda}(s) I_\lambda ds \tag{6.1}$$

where the proportionality constant is the volume extinction coefficient $\sigma_{ext,\lambda} = \sigma_{sca,\lambda} + k_{\lambda,v}$, where $\sigma_{sca,\lambda}$ is the volume scattering coefficient, and $k_{\lambda,v}$ is the volume absorption coefficient. This equation only accounts for radiation lost from incidence by extinction and does not include radiation accrued along the path by either scattering into the volume (which is described later in this chapter) or by

emission from the volume (see Section 7.1). Equation (6.1) is readily cast into a radiative transfer equation

$$\frac{dI_\lambda}{ds} = -\sigma_{ext,\lambda} I_\lambda \tag{6.2}$$

which has a solution of the form

$$I_\lambda(s'') = I_\lambda(s') \exp(-\tau_\lambda) \tag{6.3}$$

where $\tau_\lambda = \int_{s'}^{s''} \sigma_{ext,\lambda}(s) ds$ is the optical thickness. This solution is referred to as *Beer's law* and serves as the basis for the retrieval of selected atmospheric constituents integrated along the path from s' to s''. For example, consider the measurement of direct sunlight. If the sun is inclined at an angle θ_o from the vertical (the solar zenith angle), then (6.3) becomes

$$I_\lambda(\tau_\lambda^*) = I_\lambda(\tau_\lambda = 0) \exp(-\tau_\lambda^* / \cos\theta_o) \tag{6.4}$$

where τ_λ^* is the optical depth. The logarithmic form of (6.4) is

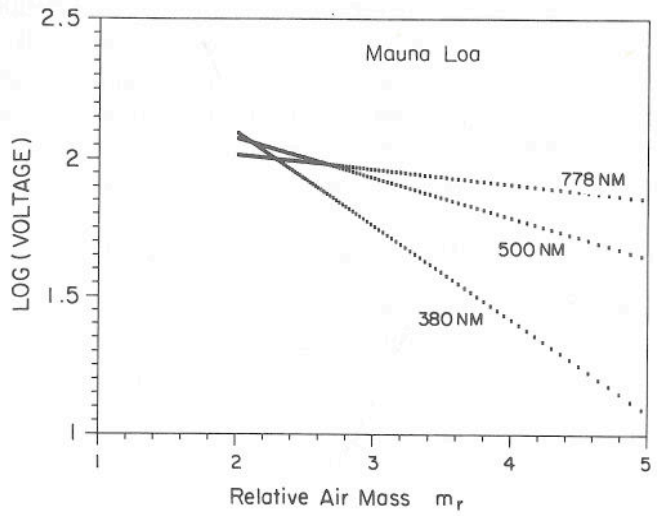

Figure 6.1 An example of a Lambertian plot for three wavelengths (in nm): the logarithm of solar intensity is plotted as a function of optical air mass for clear, stable atmospheric conditions (this air mass is $\sec\theta_o$, from Dutton, private communication).

$$\ln I_\lambda(\tau_\lambda^*) = \ln I_\lambda(\tau_\lambda = 0) - \tau_\lambda^* / \cos\theta_o \tag{6.5}$$

Figure 6.1 is an example of this type of relationship derived from radiometer measurements obtained at the Manua Loa Observatory. The data are from a spectral radiometer pointed toward the sun and measurements are recorded as the sun moves across the sky throughout the course of a day. If the logarithms of these measured intensities are plotted as a function of $\sec\theta_o$, then the optical depth τ_λ^* is the slope of the line and the incident intensity $I_\lambda(\tau_\lambda = 0)$ is given by the intercept determined by extrapolating $\sec\theta_o$ to zero.

The data presented in Fig. 6.1 indeed obey the kind of straight line relation predicted by (6.5) and this approach offers a simple and seemingly reliable way of deriving aerosol optical depths provided it is reasonable to neglect multiple scattering of sunlight and provided it is possible to remove the contributions to τ_λ^* by other constituents. The type of diagram shown in Fig. 6.1 is referred to as a *Lambertian* or *Langley* plot.

6.1.1 Aerosol Turbidity

The clear sky optical depth τ^* derived from Fig. 6.1 generally has three components. One is due to molecular scattering (Rayleigh scattering), another arises from aerosol scattering, and, depending on the wavelength in question, a third component is the absorption by certain trace gases such as ozone. The aerosol contribution is described in terms of a quantity referred to as the atmospheric *turbidity*. Measurements of this quantity have been made for about seventy years starting with Linke and Boda (1922) and Ångström (1929), and are now routinely performed worldwide as part of the World Meteorological Organization's (WMO's) solar monitoring network. The purposes of such a network include:

- determination of the "clean air" or background turbidity and the geographical, seasonal, and long–term variations of it
- detection of any unusual air pollution occurrence
- provision of information about the optical quality of the atmosphere as it relates to aerosol and gaseous pollution thereby establishing the effects of industrialization on turbidity.

There are three common definitions of turbidity. One is the turbidity index of Linke (T) which relates the total extinction in the real atmosphere to the extinction in a pure Rayleigh atmosphere by

$$I/I_o = 10^{-T\tau_{d,Ray}m_r} \tag{6.6}$$

so that

$$T = \frac{\log(I_o/I)}{\tau_{d,Ray} m_r} \tag{6.7}$$

where reference to wavelength dependences on all quantities is omitted. One way of interpreting this index is that it represents the number of Rayleigh atmospheres that must be stacked one on top of the other to produce the measured attenuation of sunlight. This index thus contains the effects of all forms of attenuation.

A second index is that of Volz (1959) which follows from (6.4) expressed as

$$I/I_o = 10^{-(\tau_{d,Ray}+\tau_{d,O_3}+B)m_r} \tag{6.8}$$

where I is the observed solar radiation at a wavelength of 0.50 μm adjusted to the mean sun–Earth distance, I_o is the solar radiation at the same wavelength outside the Earth's atmosphere at mean sun–Earth distance, $\tau_{d,Ray}$ and τ_{d,O_3} are, respectively, the decadic optical depths for Rayleigh scattering by O_2 and N_2 molecules and for absorption by ozone. The quantity B is the turbidity factor which is a measure of the aerosol optical depth. The factor m_r is referred to as the optical air mass and accounts for the slant path of the sun. This factor is approximately[1] equal to $\sec\theta_o$ for $\theta_o < 80°$.

The third turbidity index is Ångström's *turbidity coefficient* β, which is related to the aerosol optical depth according to

$$\tau_{a,\lambda} = \beta\lambda^{-\alpha} \tag{6.9}$$

where λ is the wavelength in microns and α, the wavelength exponent, is related to the aerosol particle size distribution in the manner described shortly. Rayleigh scatterers are characterized by $\alpha \approx 4$ whereas $\alpha \approx 0$ for large (relative to the wavelength) scatterers like cloud particles illuminated by sunlight. A typical value of α for atmospheric aerosol is 1.3.

6.1.2 Measurement of Turbidity

An instrument designed to measure the spectral intensity of direct sunlight at 0.50 μm and estimate B at this wavelength is the Volz sun–photometer. Another instrument used in turbidity analyses is the pyrheliometer. The first instrument of this kind dates back to

[1] The optical airmass differs significantly from $\sec\theta_o$ only when the solar elevation is low because of refraction and curvature effects on the path.

the early nineteenth century, and much of the motivation for the development of these instruments in the early part of the twentieth century stemmed from the desire to estimate the solar constant (by extrapolation of the Langley plot) and time variations of that quantity. Since then, pyrheliometers have greatly improved in their design and sensitivity, and they are currently used as a standard instrument in the WMO's global solar network. A schematic of the basic design of a pyrheliometer is shown in Fig. 6.2. The instrument consists of a thermopile [2] imbedded in an absorbing disc at the bottom of a tube with diaphragms and a limiting aperture that restricts the instrument's field of view. A filter wheel is located at the entry to the aperture. Modern pyrheliometers are often mounted on an automated sun tracker. A more detailed discussion of the operation of various types of radiometers, including pyrheliometers, is provided by Coulson (1975).

Figure 6.3 presents a time series of approximately 80 years of the Linke turbidity derived from data collected at a high altitude site far removed from the effects of urban areas. Wu et al. (1990) correlate these turbidity measurements with global and hemispheric sea surface temperatures (SSTs) obtained for the same period of time. The turbidity data suggest a slight increase in the transmittance of the atmosphere (i.e., a reduction in turbidity) throughout much of this century due to the apparent decrease in volcanic activity from the early 1900s to the 1980s. Wu et al. claim this decrease in turbidity significantly correlates with the rise in sea surface temperature over the same period of time.

Michalsky et al. (1990) analyzed a 10 year time series of turbidity data from measurements at a single site and removed the seasonal component of τ^* from this time series arguing that this variable component is representative of the tropospheric aerosol optical depth. The residual, plotted in Fig. 6.4a for the wavelength of 0.785 μm, is thus taken to be the stratospheric component of the aerosol optical depth. The various turbidity peaks correlate with

[2] Thermopiles are combinations of thermocouples configured together in some way. A thermocouple is made of two dissimilar metals that are joined. Absorption of radiation heats these metals in a dissimilar way producing a difference in temperature between the junction of the metals and a reference junction that in turn produces an electromotive force. The voltage across a single junction is small and is built up by joining several of these in series. The measured voltage is proportional to radiation incident on the thermopile.

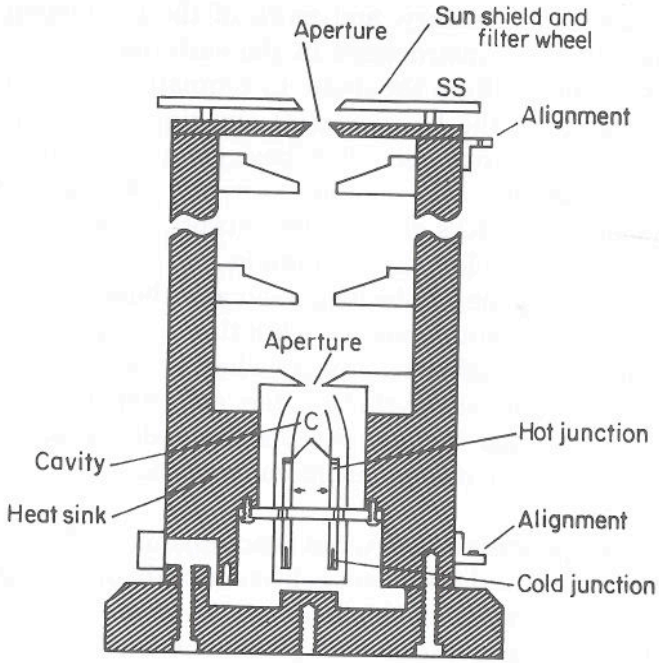

Figure 6.2 An illustration of the components of a modern pyrheliometer. A typical configuration of the filter wheel includes three filters with one aperture left open for measurement of the total spectrum.

times of volcanic activity evidenced by the prominent effects of the El Chichon eruption on the stratospheric aerosol during the early 1980s.

6.1.3 Retrieval of Particle Size

We know from the earlier discussion in Chapter 5 that the properties of extinction depend on the distribution of particle sizes within the observed volume of atmosphere. Differences in spectral measurements of particle extinction can be used to infer information about particle size distributions. To do so, however, requires some a priori information about the form of the size distribution. The simplest example of this approach is based on estimating the wavelength exponent α from measurements of τ using (6.9) and then relating this to a simple power law size distribution. To examine the method,

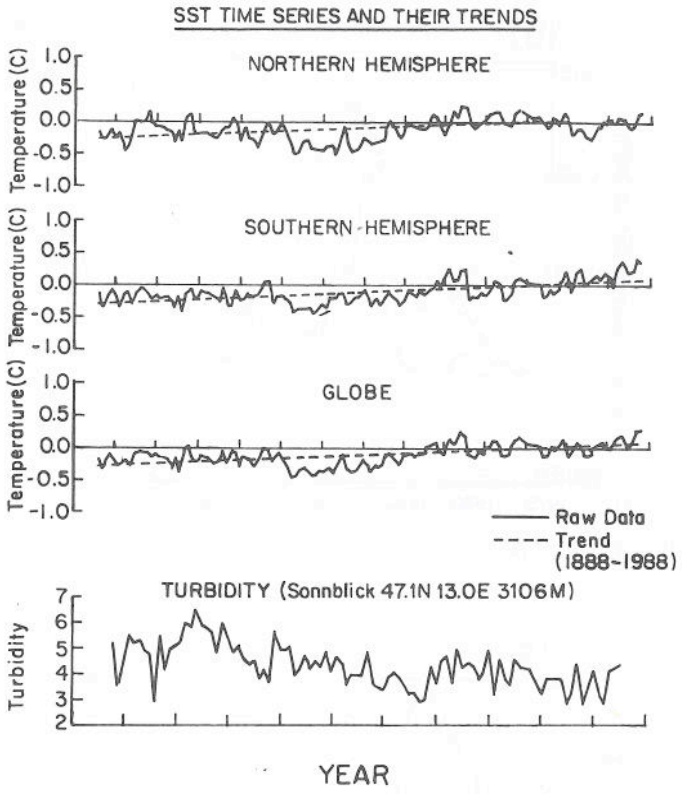

Figure 6.3 SST anomalies and trends for the northern and southern hemispheres and for the globe contrasted with the time series of Linke turbidity for a high mountain site (from Wu et al., 1990).

recall that

$$\sigma_{ext} = \int_0^\infty n(r)\,\pi r^2 Q_{ext} dr \tag{6.10}$$

is the volume extinction coefficient. The observations of Junge (1955) suggest that aerosol size distributions commonly follow a simple power law of the form

$$n(r) = \text{const}\ \ r^{-(\gamma+1)} \tag{6.11}$$

which, upon substitution into (6.10), produces

$$\sigma_{ext} = \text{const} \int_0^\infty Q_{ext} r^{1-\gamma} dr \tag{6.12}$$

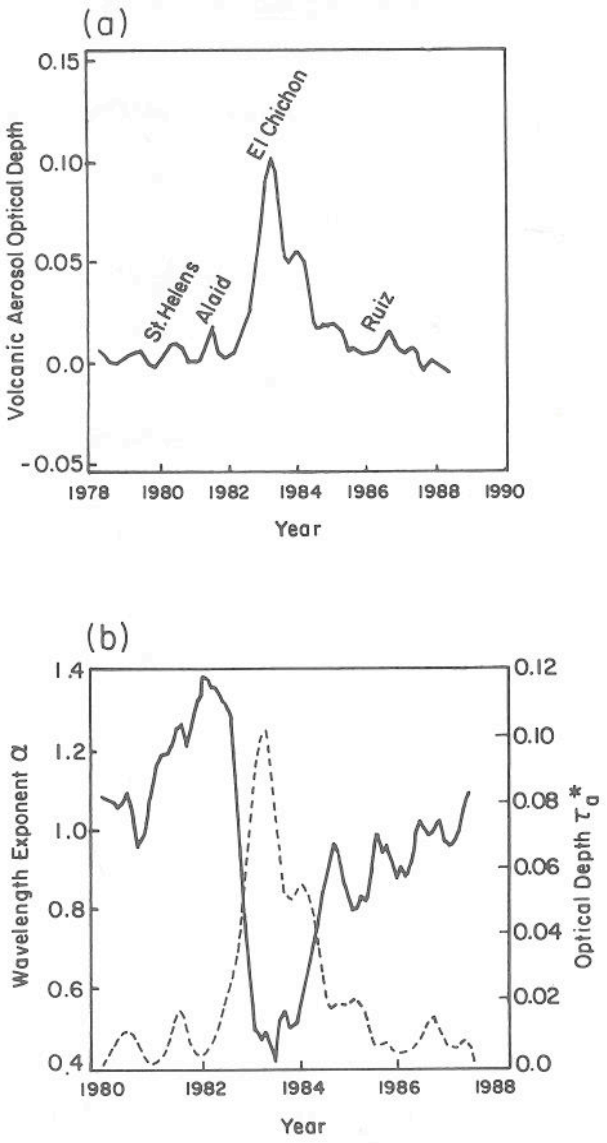

Figure 6.4 (a) Smoothed time series of volcanic aerosol optical depth perturbation at 0.785 μm. The observations were collected at a Mountain Observatory at 46.4°, 119.6°W. Volcanic events are indicated. (b) Time series of the wavelength exponent, α (solid curve) and the 0.785 μm optical depth of (a) for comparison (from Michalsky et al., 1990).

Changing the integration over aerosol size r to an integration over size parameter $x = 2\pi r/\lambda$ leads to

$$\sigma_{ext} = \text{const} \left(\frac{\lambda}{2\pi}\right)^{2-\gamma} \int_0^\infty Q_{ext} x^{1-\gamma} dx \tag{6.13}$$

If x is large and the refractive index constant with λ over the spectral range of the instrument, then Q_{ext} is approximately constant with respect to x. It follows that

$$\sigma_{ext} = \text{const } \lambda^{2-\gamma} \tag{6.14}$$

where, according to (6.9), $\alpha = \gamma - 2$.

We now introduce a basic assumption, partly for convenience, and partly out of necessity. This assumption is that the shape of the aerosol size distribution remains unchanged with height in the atmosphere so that

$$\tau_a^*(\lambda) = \text{const } H\lambda^{2-\gamma} \tag{6.15}$$

where H is a constant obtained from

$$H = \int_0^\infty h(z) dz$$

and where $h(z)$ is a normalized profile function describing the relative variation of total aerosol number density along the vertical.

The procedure for estimating α is therefore straightforward once the wavelength exponent $\alpha = \gamma - 2$ is obtained from measurements of τ_a^* at, say, two different wavelengths. The problem with this approach, as we shall see later, is that the wavelength dependence of τ_a^* is often much more complicated than predicted by the simple power law expressed by (6.15). Under these circumstances, interpretation of α is highly ambiguous. Nevertheless, this simple type of analysis offers useful qualitative information about aerosol size distributions. An example of the type of information provided by such an analysis is given in Fig. 6.4b, which shows a time series of α (solid curve) corresponding to the time series of turbidity shown in Fig. 6.4a. The aerosol optical depth shown in Fig. 6.4a is also superimposed on Fig. 6.4b for comparison. The results point to the dramatic impact of El Chichon on the mean particle size of stratospheric aerosol. At peak loading, α falls to about 0.4 implying a substantial increase in large

particles. As the El Chichon layer decays in time, the size distribution of the aerosol gradually returns to the more typical pre–eruption values of $\alpha \approx 1.3$.

Excursus: Size Distributions from Anomalous Diffraction Theory

The mathematical problem of retrieving aerosol size distributions from multispectral measurements of light extinction reduces to the problem of inverting a Fredholm integral equation

$$\tau_a^*(\lambda) = \pi H \int_0^\infty r^2 Q_{ext}(\mathrm{m}, \lambda, r) n(r) dr \qquad (6.16)$$

for the unknown function $n(r)$. $\tau_a^*(\lambda)$ is obtained from measurements of sunlight using the method described earlier in relation to (6.5) and the function $r^2 Q_{ext}$ is specified in some way. Several approximate analytical solutions to (6.16) exist for the expressions of Q_{ext}, derived from the anomalous diffraction theory formulas introduced in Section 5.5. We start with the ADT expression for a nonabsorbing wavelength written as

$$Q_{ext} = 2 - 4\frac{\sin\rho}{\rho} + 4\frac{1-\cos\rho}{\rho^2} \qquad (6.17)$$

where $\rho = k'r, k' = 4\pi(\mathrm{m}-1)/\lambda$. The inversion of this equation proposed by Fymat (1978) has the form

$$\pi r^2 n(r) = -\frac{1}{2\pi}\int_0^\infty [\cos\rho + \rho\sin\rho](\tau(k') - 2A)dk' \qquad (6.18)$$

where A, the area of the distribution, is the necessary a priori information required to invert (6.16). It is not the intention to dwell on specific methods for evaluating this equation and reference to a number of studies that address this problem are given in the notes at the end of this chapter. All methods, in principle, require extinction measurements for a large number of wavelengths (i.e., for a large number of k's). Klett (1984) introduced a general inversion to (6.16) based on the Laplace transform theory and provides a framework for coping with more practical situations that occur when measurements are made only for a limited number of wavelengths. An example of the Klett method, verified against synthetic

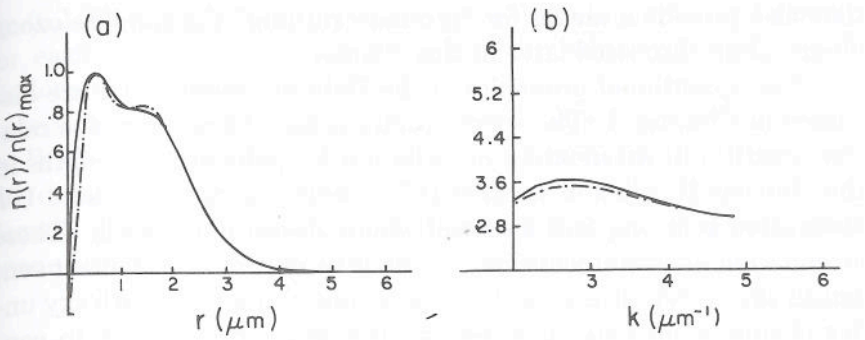

Figure 6.5 (a) Inversion of anomalous diffraction theory extinction data. The input distribution used to simulate particle extinction is plotted as a continuous line and the retrieved distribution is represented by the dashed line. (b) Anomalous diffraction, with a correction factor included (dashed), and Lorenz–Mie extinction (solid) as a function of wavenumber for the bimodal distribution in (a) (after Klett, 1984).

distributions, is given in Fig. 6.5a by the dashed line. Ten extinction values were selected to resolve the $\tau - k'$ spectrum which is also shown in Fig. 6.5b for reference. This is a more complex spectrum than typically predicted by Ångström's turbidity formula (6.9) and is a result of the more complicated bimodal size distribution used to generate the spectrum. The Klett retrieval appears at least capable of reproducing this bimodality.

6.2 More on Extinction–Based Methods

6.2.1 Total Ozone from UV Extinction Measurements

During the 1970s a surge of public concern surfaced about partial destruction of the ozone layer due to anthropogenically produced pollutants. Since then, the substantial depletion of ozone over the Antarctic during the southern hemisphere springtime months was discovered. This has led a significant push into research on ozone chemistry. In recognition of the pressing need for a coordinated international ozone monitoring network, in the 1970s the WMO initiated a special effort to enhance the existing global ozone network. The Dobson ozone spectrometer was selected as the instrument for this worldwide network. Not only do these measurements serve the important purpose of determining hemispheric and global ozone trends,